PHYSICAL REVIEW B **92**, 165203 (2015)

Complexes of silicon, vacancy, and hydrogen in diamond: A density functional study

Gergő Thiering and Adam Gali

Wigner Research Center for Physics and Optics, Hungarian Academy of Sciences, P.O. Box 49, H-1525 Budapest, Hungary
and Department of Atomic Physics, Budapest University of Technology and Economics, Budafokiút 8, H-1111 Budapest, Hungary

(Received 10 September 2015; published 20 October 2015)

Paramagnetic luminescent point defects in diamond are increasingly important candidates for quantum information processing applications. Recently, the coherent manipulation of single silicon-vacancy defect spins has been demonstrated in chemical vapor deposited diamond samples where silicon may be introduced as a contamination in the growth process. Hydrogen impurity may simultaneously enter diamond too and form complexes with silicon-vacancy defects. However, relatively little is known about these complexes in diamond. Here we report plane-wave supercell density functional theory results on various complexes of silicon vacancy and hydrogen in diamond. We found a family of complexes of silicon, vacancies, and hydrogen atoms that are thermally stable in diamond with relatively low formation energies that might form yet unobserved or unidentified silicon-related defects. These complexes often show infrared optical transitions and are paramagnetic. We tentatively assign one of these complexes to a recently reported but yet unidentified infrared absorber center. We show that this center has a metastable triplet state and might exhibit a spin-selective decay to the ground state, thus it is an interesting candidate for quantum information processing applications. We also discuss here methodology aspects of calculating hyperfine parameters and intradefect level excitations in systems with notoriously complex electron states within hybrid density functional approach. We also demonstrate that a simplified approach using *ab initio* data can be very powerful to predict the relative intensities of the phonon replica associated with quasilocal vibration modes in the photoexcitation spectrum.

DOI: 10.1103/PhysRevB.92.165203 PACS number(s): 71.15.Mb, 61.72.Bb, 71.55.Ht

I. INTRODUCTION

High quality diamond crystals are grown by chemical vapor deposition (CVD) technology where the carrier gas is hydrogen and silicon contamination often occurs in the CVD chamber. As a consequence, silicon-related defects can appear in CVD diamonds. Nevertheless, the knowledge about silicon-related point defects and complexes is scarce. The most known silicon-related defect is the so-called silicon-vacancy center (SiV) [1]. We note that SiV defects were reported in gem diamonds and nanodiamond meteorites too [2–4]. This is an exceedingly important defect as its electron spin can be coherently manipulated by light and it is an important candidate in various quantum information processing applications [5,6]. The microscopic structure of this defect was identified by *ab initio* density functional theory (DFT) calculations [7,8]. This defect was observed in two different charge states: the 1.682-eV photoluminescence (PL) center with $S = 1/2$ spin is associated with the negatively charged SiV defect [SiV(−)] [7,9–12] whereas the 1.31-eV PL center with $S = 1$ spin is associated with the neutral SiV defect [SiV(0)] [10,13]. The KUL1 electron paramagnetic resonance (EPR) center has been identified as SiV(0) [10,13]. Upon high-temperature annealing the intensity of the 1.682-eV PL line increases and of the 1.31-eV PL line decreases in diamond [13,14] which might be interpreted that the Fermi-level shifts up in this process stabilizing the negative charged state of the defect. Recent secondary ion mass spectroscopy (SIMS) measurements indicate [14,15] that other silicon-related defects should occur in diamond as the estimated concentration of SiV defects was much smaller than the total concentration of Si impurities in the studied diamond samples. The formation energy of substitutional and interstitial Si is high due to the tight diamond lattice, thus the formation of larger silicon vacancy complexes with the naturally present hydrogen impurities were considered by DFT calculations [16,17]. It was shown that a diffusing vacancy favorably forms a complex with SiV defect [16] that we label SiV_2 defect. We note here that *ab initio* calculations revealed [18] that the positively charged interstitial hydrogen is mobile in diamond and can thus form complexes with various defects [18–26]. The complex formation of a single hydrogen with SiV and SiV_2 defects, i.e., SiV:H and SiV_2:H defects, respectively, was also found to be favorable by DFT calculations [16,17]. In addition, the formation of SiV complex with two hydrogen atoms ($SiV:H_2$ defect) was also considered [16]. The appearance of silicon-vacancy-hydrogen complexes was indeed demonstrated. The KUL3 EPR center [27] was successfully identified as the neutral SiV:H defect [15,16] and the WAR3 EPR center as the neutral SiV_2:H defect [17] based on the measured and calculated hyperfine signals. However, no evidence of complexes with two or more hydrogen atoms within silicon-vacancy centers has been demonstrated so far in diamond. We note here that an absorption line at 1.018 eV was found in CVD diamond (page 151 in Ref. [14]) after high-temperature anneal at around 2000 °C where the KUL3 and WAR3 EPR signals disappeared and the relative intensity of SiV(−) PL signal increased with respect to that of SiV(0) PL signal. Since the 1.018-eV absorption line was found in silicon contaminated CVD diamond it might be associated with an unidentified silicon-related defect. This absorption center might be related to a ∼0.92–1.05-eV thermoluminescence center in CVD diamond film grown on Si substrate that was cleaned by hydrogen plasma [28–30].

In this paper we systematically study the complexes of multiple hydrogen atoms with SiV and SiV_2 defects in

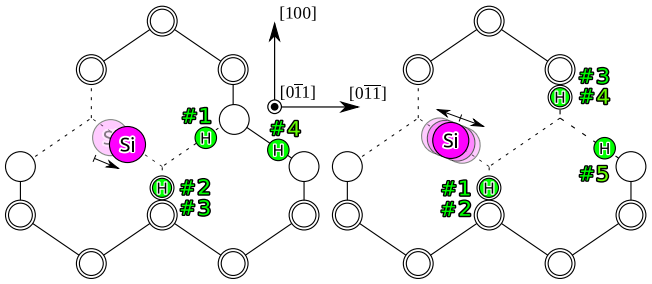

FIG. 1. (Color online) Schematic geometry of the considered defects. The double circles mark two atoms that are out of the (110) mirror plane and symmetrically equivalent. The subfigure on the left side is a SiV defect decorated with H atoms, and on the right-hand side H atoms are added into the SiV_2 complex. The green numbers label the position of the H atoms in these complexes. Symmetrically equivalent H atoms are also depicted by double circles. The purple balls labeled by Si show the position of the Si atom in the defect. In SiV:H_n complex the arrow schematically represents the typical geometry distortion upon optical excitation of the defect whereas the left-right arrow in the SiV_2:H_n complex represents the motion of Si atom in a typical Si-related vibration mode along [111] direction. This type of quasilocal vibration mode is expected to appear as vibration replica in the optical signals.

diamond (see Fig. 1) by *ab initio* supercell plane-wave density functional theory calculations. We find that the formation energies of these complexes are relatively low and the binding of hydrogen atoms to these complexes is favorable. We calculated the optical signals as well as the EPR signals of these defects at the fully *ab initio* level to mediate the future identification of these complexes. We tentatively assign the negatively charged SiV:H defect to the 1.018-eV absorption center. Our calculations reveal that this defect might be an interesting candidate for realizing a long-living quantum memory in diamond.

The paper is organized as follows. In Sec. II we describe the applied methods in detail. In Sec. III we present the results of the atomistic simulations for SiV and SiV_2 related complexes. Some of these complexes possess highly correlated electron states. We briefly discuss the hybrid density functional theory in this context and provide practical approaches to calculate the different physical quantities. In a separate section (Sec. IV) we discuss the assignment of the 1.018-eV absorption center to the considered silicon-vacancy-hydrogen complexes in detail. Here we calculate *ab initio* the phonon replica in the absorption center where the methodology is described in the Appendix. Finally, we conclude our paper in Sec. V.

II. METHODOLOGY

We apply plane-wave supercell spin-polarized density functional theory calculation on the complexes of silicon, vacancy, and hydrogen in diamond as implemented in the VASP code within the Born-Oppenheimer approximation where the nuclei are classical ions and the electrons are treated explicitly [31,32]. We use a relatively large 512-atom simple cubic supercell that allows us to sample the Brillouin zone at the Γ point. At the Γ point the degeneracy of the Kohn-Sham wave functions can be monitored and the convergent charge and spin densities can be simultaneously obtained in the applied supercell. The ions are treated within the projector augmentation wave (PAW) method [33] which makes possible a relatively low-energy cutoff for the expansion of the plane waves and accurately calculates the charge and spin densities at the ion positions.

The applied DFT functionals and plane-wave cutoffs are optimized for the considered physical quantities and computational capacity. We applied the Perdew-Burke-Ernzerhof (PBE) generalized gradient approximated variant of DFT [34] to calculate the ground-state charge and spin densities as well as the phonons of the systems. In this case we use the PBE optimized lattice constant of the supercell (3.570 Å). The choice of PBE for calculating the phonons is motivated by two reasons: (i) PBE very accurately reproduces the experimental diamond lattice constant, phonon spectrum, and the dependence of these properties of pressure or temperature [35]; (ii) as we allow all the atoms to vibrate it would be computationally prohibitive to apply nonlocal functionals to obtain the results. In the VASP implementation within density functional perturbation theory [36] the calculated Raman mode at 1326 cm^{-1} in our 512-atom supercell is in very good agreement with the experimental data of 1332 cm^{-1} [37]. In the defective calculations, we allowed all the atoms to relax until the forces fall below the threshold of 10^{-4} eV/Å. This strict limit for the forces is particularly needed for accurate calculation of the vibration modes. We applied inverse participation ratio (IPR) analysis to study the localization of the vibration modes [38] where larger IPR values indicate stronger localization. The plane-wave cutoff was set to 370 eV in these calculations that was already proven to be convergent for the SiV defect [10]. The zero-field splitting upon electron-spin–electron-spin interaction, the so-called D tensor, was also calculated within this framework that we have recently implemented and provided good agreement with the experiment for the nitrogen-vacancy center in diamond [39].

The charge transition levels as well as the intradefect level optical transition energies were determined by HSE06 [40,41] screened hybrid functional because it provides quantitatively good agreement for defects in diamond [42–44] including the SiV center [10]. In this case the optimized lattice constant is 3.545 Å. We applied the ΔSCF method to calculate the excited states of the system that allows us to calculate the potential-energy surface in the excited state, thus the zero-phonon-line (ZPL) energies can be determined and compared to the experimental data [10,42]. The applied plane-wave cutoff was set to 370 eV except in the calculations of hyperfine couplings between the electron and nuclei spins where the cutoff was raised up to 600 eV. We calculated the hyperfine couplings including the core spin polarization in the Fermi-contact interaction within the frozen valence approximation [45] as implemented in the VASP code [46].

We calculated the formation energy $[E_f^q(E_F)]$ of various defects of charge state q as a function of the Fermi level E_F in the fundamental band gap by following the definition of Zhang and Northrup [47],

$$E_f^q(E_F) = E_{tot}^q - \sum_{C,Si,H} n_i\mu_i - q(E_F - E_V) + \Delta E_{corr}^q, \quad (1)$$

TABLE I. Summary of binding energies of the most stable complexes of silicon, hydrogen, and vacancies as described in Eq. (3) with the chosen Fermi level of $(E_F - E_V) = 1.5$ eV. Such charge state was chosen in the calculation of the formation energy for a given defect that is the most stable at this Fermi level. The corresponding geometries are shown in Fig. 2.

SiV	H	H_2	H_3	H_4	
Symmetry	C_s	C_s	C_{3v}	C_s	
Binding energy (eV)	4.82	4.10	2.78	2.15	
SiV_2	H	H_2	H_3	H_4	H_5
Symmetry	C_s	C_s	C_s	C_1	C_s
Binding energy (eV)	6.07	5.48	5.26	4.37	2.91

where μ_{Si} and μ_C values are the chemical potential of silicon and carbon atoms in the diamond lattice. The value of μ_C is the total energy of the perfect diamond lattice per atom whereas μ_{Si} was deduced from the ultimate limit of Si-rich diamond forming cubic silicon carbide (SiC). The chemical potential of hydrogen is taken from the hydrogen molecule in an appropriate large vacuum unit cell. Here we did not try to simulate realistic growth conditions but rather we considered the relative formation energies of hydrogen-related defects. The Fermi level E_F is referenced to the calculated value of the valence-band maximum (VBM) of the perfect diamond lattice (E_V). Finally, ΔE^q_{corr} is the total-energy correction of the defective charged supercell. Here, we applied a relatively simple formula, 2/3 of the monopole term of the Makov-Payne correction [48,49] after average potential correction, which practically yields equivalent results with the Freysoldt correction [50,51] and is able to properly reproduce the experimental ionization energies of deep defects in group-IV crystals [43] including the defects in diamond [10,44] within the accuracy of about 0.1 eV.

The adiabatic charge transition levels for a single defect $E(q|q+1)$ can be derived from Eq. (1) and are calculated as

$$E(q|q+1) = E^q_f - E^{q+1}_f = E^q_{tot} - E^{q+1}_{tot} + \Delta E^q_{corr} - \Delta E^{q+1}_{corr}, \quad (2)$$

which yields the position of the Fermi level where the formation energy of the defect for the two charge states q and $q+1$ are equal.

We also calculated the binding energy of hydrogen atom in hydrogen-related defects. In this model we assume a mobile interstitial hydrogen (H_{BC}) that can be trapped by $SiV{:}H_n$ or $SiV_2{:}H_n$ complexes forming $SiV{:}H_{n+1}$ and $SiV_2{:}H_{n+1}$ complexes, respectively. We explicitly write here the applied equation for the binding energy E_{bind} of $SiV{:}H_n + H_{BC} \rightarrow SiV{:}H_{n+1}$ reaction:

$$E_{bind} = E^{q_2}_f(SiV{:}H_n) + E^{q_3}_f(H_{BC}) - E^{q_1}_f(SiV{:}H_{n+1}) + \sum_{j=1}^{3} q_j E_F. \quad (3)$$

In this definition, positive binding energy means favorable reaction and a larger value of E_{bind} indicates a larger probability of reaction where this depends on the actual position of E_F which sets the stable charge states (q_j) of the defects in the reaction. We will show that experiments indicate [14,17] that the Fermi-level pins close to the $(0|-)$ charge transition level of SiV defect in diamond which is around at $E_V + 1.5$ eV [10]. Thus, we set E_F accordingly in the calculation of binding energies where H_{BC} is positively charged (see Fig. 3), i.e., $q_3 = +1$ in Eq. (3), and it is indeed mobile in this charge state in diamond [18].

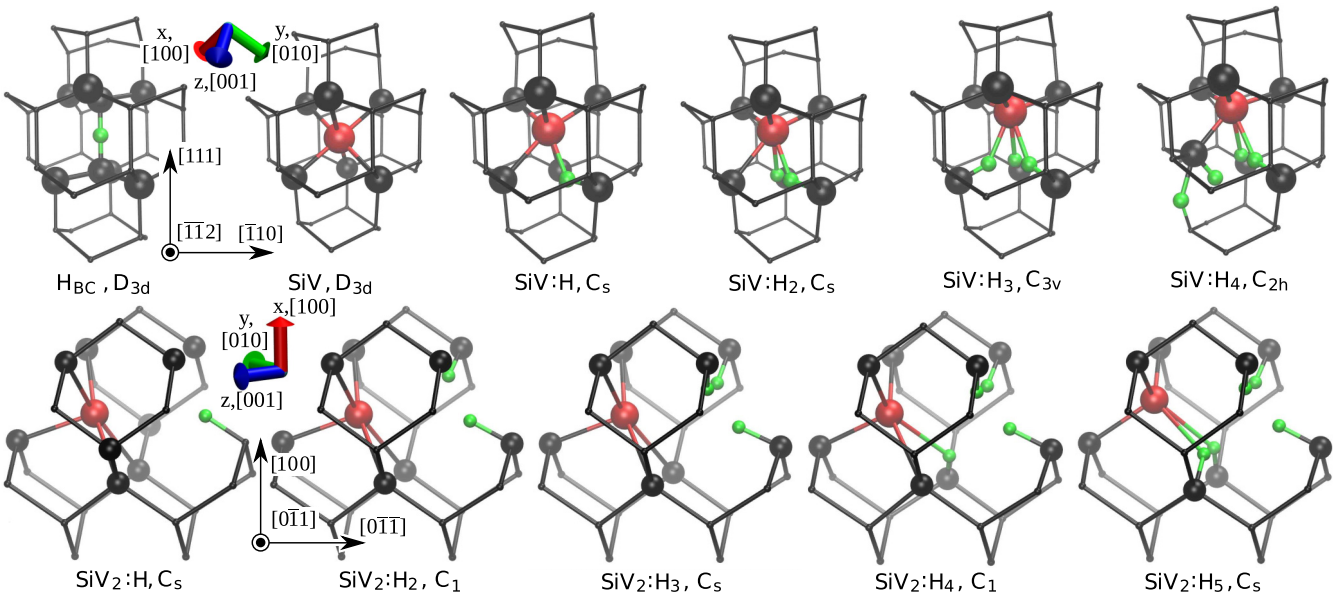

FIG. 2. (Color online) Relaxed geometries of the considered complexes extracted from 512-atom diamond supercell. The black balls represent the six nearest-neighbor (NN) C atoms in SiV-related complexes and 8 NN C atoms in SiV_2-related complexes next to silicon atom, also more distant C atoms are in the intersection of the black wires. The Si atom is represented by a large red ball and the H atoms by small green ones. The point-group symmetry for each defect system is also depicted.

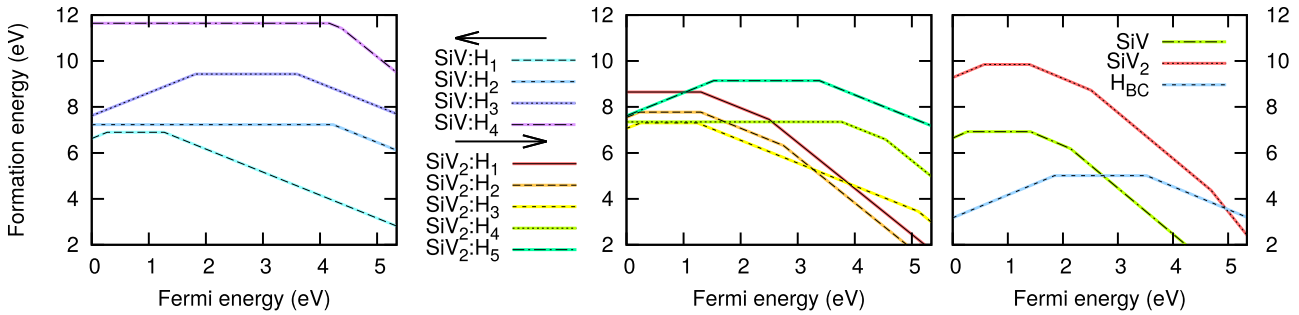

FIG. 3. (Color online) Formation energies of the considered complexes as a function of the Fermi level [see Eq. (1)]. The origo of the Fermi level is aligned to the top of the valence band. The change in the steepness of the curves gives the corresponding charge transition levels for a single defect. H_{BC} labels the interstitial hydrogen in the diamond lattice.

III. RESULTS

We systematically investigated SiV and SiV_2 complexes with hydrogen atoms. The binding energy of hydrogen atoms to these defects is shown in Table I and the corresponding optimized geometries are depicted in Fig. 2. One may infer from Table I that complexes of four hydrogen atoms with SiV defect and of five hydrogen atoms with SiV_2 defect may occur, respectively. Complexes of larger number of hydrogen atoms are not favorable according to the calculated binding energies. In addition to the binding energies, we calculated the formation energies of these complexes as a function of the Fermi level in the gap (see Fig. 3) where we aligned the reference of the Fermi level to the top of the valence band. We will use this reference in the rest of the paper. From these plots one can conclude that complexes of one or two hydrogen atoms with SiV defect and of one, two, or three hydrogen atoms with SiV_2 defect are stable at a realistic position of the Fermi level, although $SiV:H_3$, $SiV_2:H_4$, and $SiV_2:H_5$ cannot be entirely excluded based on this ground in p-type diamond. Thus, we will discuss SiV:H, $SiV:H_2$, SiV_2:H, $SiV_2:H_2$, $SiV_2:H_3$ complexes in detail in the next sections whereas we only briefly summarize the results for the $SiV:H_3$, $SiV_2:H_4$, and $SiV_2:H_5$ complexes.

A. Silicon-vacancy defect with a single hydrogen atom: The SiV:H defect

It is intriguing to start the investigation of SiV:H defect with the ancestor split silicon-vacancy defect in order to understand its electronic structure. The SiV defect has been recently investigated by HSE06 DFT plane-wave supercell calculations [10], thus we do not reiterate the results here. We briefly mention that the SiV defect has high D_{3d} symmetry where the Si atom sits in the inversion center and the six nearest-neighbor carbon atoms have single dangling bonds. The neutral SiV defect has a double degenerate e_g state in the gap occupied by two electrons forming a high $S = 1$ spin state [7,10–12]. A single hydrogen atom can terminate one of the carbon dangling bonds with lowering the symmetry to C_s. As a consequence, the e_g level splits to a' and a'' levels. The hydrogen atoms add an electron to the SiV defect, thus these levels are filled by three electrons. According to HSE06 calculations, the symmetric a' is fully occupied and its level falls below the valence-band maximum. The asymmetric a'' becomes half occupied and its level appears in the gap forming a $S = 1/2$ spin state. We will refer to these Kohn-Sham orbitals as $1a'$ and $1a''$ states in the context (see Fig. 4). Another localized state appears resonant with the conduction band that

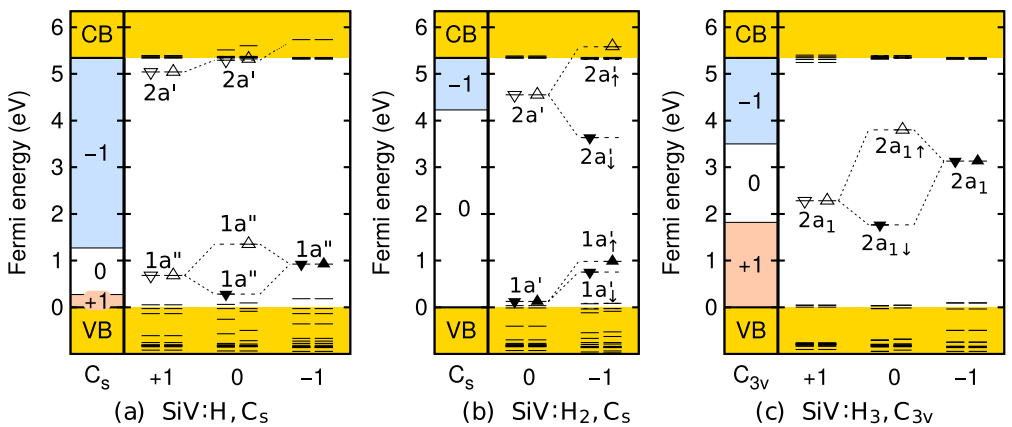

FIG. 4. (Color online) Charge transition levels and localized Kohn-Sham levels within the diamond gap for selected $SiV:H_n$ defects. All results are obtained by HSE06 hybrid functional. The filled (unfilled) triangles represent occupied (unoccupied) states. The spin-up and spin-down channels are shown separately, as symbolized with the orientation of the triangle. Due to spin-polarized calculations the spin-up and spin-down states may split in energy.

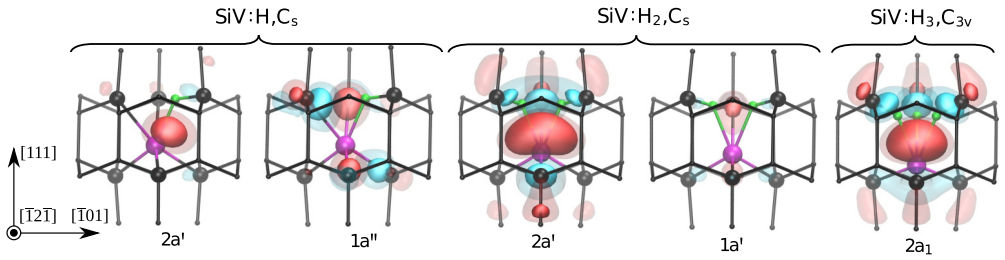

FIG. 5. (Color online) Visualization of Kohn-Sham wave functions of selected SiV:H_n defects. All the states are the corresponding down-spin components in their neutral charge state. The opaque red and blue lobes represent the wave function with an isovalue of ± 0.025 while the transparent ones represent the wave function with an isovalue of ± 0.015.

we label as $2a'$. This state is originated from the interaction of Si and H atom as shown in Fig. 5.

The electronic structure of neutral SiV:H defect implies that single positively and negatively charged SiV:H defects may exist in diamond. The $(+|0)$ charge transition level is very close to the valence-band edge and not very likely to occur, however, the $(0|-)$ level is at $E_V + 1.27$ eV, thus its acceptor level lies deeper than that of the SiV defect but not too far from it. The negatively charged SiV:H defect has a fully occupied very deep level in the gap, thus it might be optically excited with ultraviolet (UV) light. However, the neutral SiV:H defect may be optically excited by near-infrared (NIR) light and it has been associated with the KUL3 EPR center [17]. Thus, we discuss the neutral SiV:H defect in detail.

We start with the discussion of the magnetic properties of the defect. We calculated the hyperfine tensors for the ^{1}H and ^{29}Si nuclei with different functionals for comparison with previous DFT results (see Table II). The hyperfine parameters obtained by the HSE06 method overestimates the experimental values for ^{29}Si nuclei. The hyperfine constants of ^{29}Si are due to the overlap of the nearest-neighbor carbon dangling-bond orbitals that spin polarize the electron density around the Si nucleus. This indirect spin polarization is very sensitive to the distance between atoms. HSE06 a bit underestimates the lattice constant of diamond in our implementation which results in a bit larger overlap between Si and the carbon dangling-bond orbitals, hence the overestimation of the ^{29}Si hyperfine constants. We have the same experience with the neutral SiV defect associated with the KUL1 EPR center [10]: the experimental hyperfine values of ^{29}Si nucleus are ($A_\parallel = 76.3$ MHz, $A_\perp = 78.9$ MHz [15]) compared to HSE06 values of ($A_\parallel = 92$ MHz, $A_\perp = 97$ MHz), however, the ^{13}C hyperfine constants were accurately reproduced [10]. Thus we expect the overestimation for the ^{29}Si hyperfine constants in SiV:H defect too. We note that our HSE06 calculations consistently reproduce the order of the highest and the lowest hyperfine constants on the ^{29}Si nucleus. This is in contrast with the results of PBE calculations where we also compare our results with previously reported ones [17]. In order to be consistent with the previous study, we do not apply the core-polarization correction in the hyperfine constants by the PBE method. The magnitude of this correction is about 1 MHz for ^{29}Si nuclei. The differences between our PBE results and the previously reported ones [17] might be related to a different basis set (s and p Gaussians vs plane waves) and treatment of the core electrons (norm-conserving pseudopotentials vs PAW formalism). The PBE functional delocalizes the defect states so the spin density that leads to the underestimation of the hyperfine tensor as was explained in our previous study [46].

TABLE II. Hyperfine parameters in SiV:H defect from experiments and *ab initio* simulations. The directions for each main axis of the hyperfine tensors are shown in Fig. 6. We provide the direction of hyperfine constants in parentheses in spherical coordinates (ϑ and φ angles, respectively). ϑ is the angle from [001] while φ is the angle from [100] in a (001) plane.

	Type	A_{xx} (MHz)	A_{yy} (MHz)	A_{zz} (MHz)
Expt.[a]	^{1}H	−7.9 (130,45)	4.7 (40,45)	7.3 (90,315)
	^{29}Si	76 (53,45)	81 (143,45)	79 (90,315)
PBE[a]	^{1}H	−7.0 (133,45)	3.0 (43,45)	6.0 (90,315)
	^{29}Si	88 (55,45)	86 (145,45)	89 (90,315)
PBE	^{1}H	−6.2 (134,45)	1.5 (44,45)	5.0 (90,315)
	^{29}Si	53.9 (27,45)	54.7 (117,45)	55.2 (90,315)
HSE06	^{1}H	−6.4 (127,45)	2.8 (37,45)	10.2 (90,315)
	^{29}Si	110 (49,45)	118 (139,45)	116 (90,315)

[a]Reference [17].

To our best knowledge, no absorption or PL center has been associated with the neutral SiV:H defect. The calculated ZPL is at 0.95 eV, thus it should be in the near-infrared region like for the neutral SiV defect. This excitation promotes a spin-up electron from a level below the valence-band edge to the unoccupied spin-up defect level in gap. In the excited state the unoccupied Kohn-Sham level shifts above the valence-band edge which is mostly localized to one dangling bond while the occupied state is localized to the first neighbor C atoms near the Si atom excluding the C-atom forming the C-H bond.

We also calculated the vibration spectrum of this defect that might be detected in the infrared absorption spectrum or a phonon sideband in the absorption or luminescence spectrum. In a previous DFT PBE study [16], a C-H stretch mode at 3092 cm^{-1} and a C-H bending mode at 1740 cm^{-1} were reported that both belong to the a' representation in C_s symmetry. We report these values at 3197 and 1655 cm^{-1}. The second bending mode with a'' character is smeared into the diamond phonon band at approximately 900–1000 cm^{-1}. We found quasilocal vibration modes with IPR analysis that are associated with the motion of the Si atom at 301 cm^{-1} (0.03) and at 343 cm^{-1} (0.28), where the values in the parentheses are the IPR values for each vibration. Both of these vibration modes originate from the Si vibration along the [111] direction,

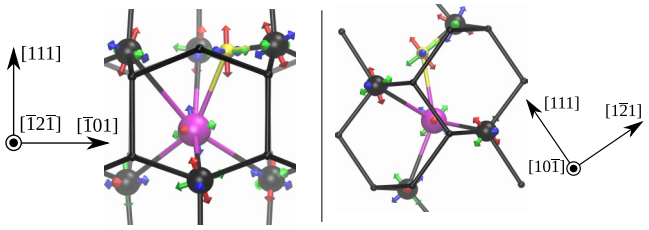

FIG. 6. (Color online) The hyperfine couplings in the SiV:H defect. The red, green, and blue arrows represent the direction cosine of the hyperfine values A_{xx}, A_{yy}, and A_{zz}, respectively. The list of hyperfine constants are tabulated in Table II.

i.e., along the D_{3d} high-symmetry axis of the ancestor SiV defect. This [111] direction is only approximate because of the presence of the H atom that distorts the D_{3d} symmetry. We found two other quasilocal modes where the motion of the Si atom is perpendicular to the [111] direction. Along the [$2\bar{1}\bar{1}$] direction a quasilocal mode appears at around 480 cm^{-1} with a' symmetry. The third a'' vibration mode along the [$01\bar{1}$] is at 470 cm^{-1}.

B. Silicon-vacancy defect with two hydrogen atoms: The SiV:H$_2$ defect

We calculated multiple configurations of SiV:H$_2$ complexes. The system with C_s symmetry with two hydrogen atoms placed nearest to each other was the lowest energy configuration (see Table III). We simply label this configuration as C_s in the context.

We now discuss the electronic structure of the most stable configuration. Two localized states appear in the gap: a fully occupied $1a'$ and an empty $2a'$ in the neutral charge state. The lower-lying one is the descendant state of the split e_g state of the SiV defect, however, in contrast to the case of the SiV:H defect, the $1a''$ state falls in the valence band whereas the $1a'$ state lies above but very close to the valence-band edge. The higher-lying one is now discussed in detail that is localized near Si, H, and such C atoms that bond to hydrogen. This state may be defined as a "nonbonding" or "antibonding" state because the wave function changes its sign at the place of H atoms resulting in a different sign around the Si atom and the corresponding C atoms; see Fig. 5. This type of bonding is known as electron deficient bonding, reported in the diborane molecule [52], that was later found in X-H-X linear systems [53], and more recently has been reported in a solid-state system [54]. We note that the same type of bonding appears in the SiV:H and the SiV:H$_3$ defect (see Fig. 5). In the SiV:H defect this state is resonant with the conduction band thus it is not so visible, therefore we discussed the nature of this state in the SiV:H$_2$ defect.

We found that only the neutral and negatively charged SiV:H$_2$ defects are stable in diamond where the $(0|-)$ level is at $E_V + 4.23$ eV. The electronic structure of the defect implies that the defect has no visible optical transition. However, the defect is rich in local and quasilocal vibration modes that might be detected in infrared absorption measurements. A previous study found local vibration modes at 3480 and 3240 cm^{-1} (symmetric a' and antisymmetric a'' stretch modes, respectively) as well as bending modes at 1520 and 1400 cm^{-1}, both with a' character [16]. We report these features at 3460, 3245, 1505, and 1375 cm^{-1}, respectively. The remaining two bending modes with a' and a'' characters fall into the diamond phonon band at approximately 900 ± 100 cm^{-1}. The modes involving the Si atom are at 361 cm^{-1} (a' symmetry along the [111] direction) and the others are at 462 cm^{-1} (a' symmetry along the [$2\bar{1}\bar{1}$] direction) and 493 cm^{-1} (a'' symmetry along the [$01\bar{1}$] direction). These quasilocal modes smear in the phonon sideband with a distribution of about ± 30 cm^{-1}.

TABLE III. The relative stability of SiV:H$_2$ complexes from HSE06 calculations in the negative and neutral charge states. The calculated total energy is referenced to the most stable defect, the SiV:H$_2$ defect with C_s symmetry.

	Energy (eV) of different configurations		
Charge state	C_s	C_1	C_{2h}
$(-)$	0.00	1.16	1.84
(0)	0.00	0.77	1.28

C. Silicon-vacancy defect with three hydrogen atoms: The SiV:H$_3$ defect

We briefly discuss here the complex of three hydrogen atoms with the SiV defect that might appear in heavily hydrogenated diamond samples. The most stable configuration has C_{3v} symmetry as depicted in Fig. 2. Only the $2a_1$ state appears in the gap that arises from electron deficient bonding as was explained in the SiV:H$_2$ defect. In the neutral charge state a single electron occupies this state forming an $S = 1/2$ EPR active ground state. By removing and adding an electron to the system positively and negatively charged defects may form, respectively. The calculated $(+|0)$ and $(0|-)$ levels are at $E_V + 1.82$ eV and $+3.60$ eV, respectively.

We focus our attention to the paramagnetic neutral state. We found a large hyperfine coupling with the ^{29}Si nucleus: $A_{\parallel} = -608$ MHz and $A_{\perp} = -388$ MHz. This is very characteristic for this defect and is caused by the lobes of the three Si-H bonds. We also calculated the vibration modes for this defect. The highest mode is at 3541 cm^{-1} with a_1 character. The next mode is a double degenerate e mode at 3203 cm^{-1}. These modes explain the three C-H stretch modes. We found the C-H bending modes at 1423 cm^{-1} (e) and 1398 cm^{-1} (a_1). The remaining e and one a_2 bending modes are hybridized with the diamond phonons near 800–1000 cm^{-1}. The quasilocal modes associated with the motion of the Si atom are at around 299 cm^{-1} (a_1) and 356 cm^{-1} (e).

D. Complexes of two vacancies with silicon: The SiV$_2$ defect

Silicon may form complexes with two vacancies [16] that can be described as a SiV defect adjacent to a second vacancy (see Fig. 7). As a consequence, some states may be derived from the SiV defect and other states from the carbon dangling bond of the second vacancy. We obtained three defect states in the band gap by HSE06 calculations. The $1a''$ is the deepest defect state which is a descendant of the e_g states of the SiV defect. The other $2a'$ and $2a''$ orbitals are localized near the second vacancy, i.e., three carbon dangling bonds (see Fig. 10).

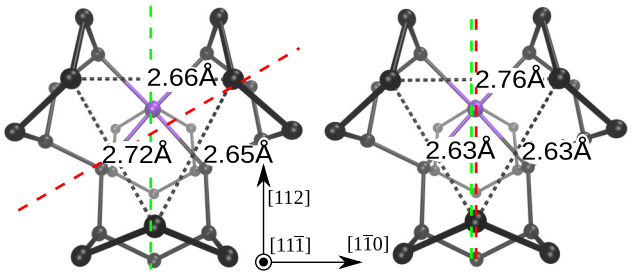

FIG. 7. (Color online) The geometry distortion of the negatively charged SiV_2 defect. The purple ball depicts the Si atom. The three values show the C-C distances in the second vacancy. The green lines represent the mirror plane involving the Si atom along the Si-V-V chain. The red lines represent the local mirror plane of the three C atoms nearest to the second vacant site. According to our results, the configuration on the left is energetically favorable over the configuration on the right by 0.12 eV.

We use the same labeling of these defect states in SiV_2:H_n complexes.

The HSE06 defect levels are plotted in Fig. 8. In the neutral charge state the $1a'$ orbital is fully occupied whereas the $2a'$ and $2a''$ orbitals are empty which form a singlet ground state. We note that these multiple states in the gap imply complex absorption peaks in the near-infrared region. According to our calculation the defect might exist in the positive, neutral, negative, doubly negative, and triply negative charge states, however, the positive and triply negative charged defects do not likely occur in usual diamond samples. The electronic structure and geometry of the $SiV_2(-)$ defect need further discussion. The extra electron occupies the $2a'$ state originated from the dangling bonds of the second vacancy. This results in a pseudo-Jahn-Teller effect as shown in Fig. 7: the "local" C_{3v} symmetry of the second vacancy is broken which leads

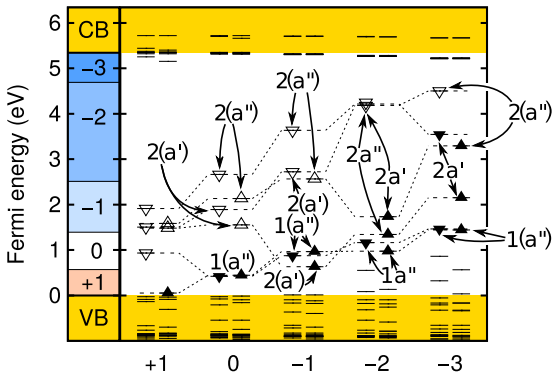

FIG. 8. (Color online) Charge transition levels and Kohn-Sham defect levels in the band gap of diamond for SiV_2 defect. All results are obtained with HSE06 hybrid functional. The filled triangles represent occupied electrons whereas unfilled ones represent empty states. The spin-up and spin-down channels are shown separately, as symbolized by the orientation of the triangle. Due to spin-polarized calculations the spin-up and spin-down states may split in energy. Strictly speaking, the $(-)$ state does not show C_s symmetry (see Fig. 7) but we still label the corresponding Kohn-Sham orbitals as descendants from C_s symmetry.

to a very low C_1 symmetry of the entire SiV_2 complex. The energy gain compared to the C_s configuration is 0.12 eV.

E. Complex of SiV_2 defect with a single hydrogen atom: The SiV_2:H defect

By adding one hydrogen to the SiV_2 defect it should terminate one of the carbon dangling bonds. According to HSE06 calculations, the most favorable configuration possesses C_s symmetry and the hydrogen goes to the second vacancy. The localization of the resulting defect states in the gap is shown in Fig. 10. In the neutral charge state of the defect, a $2a'$ level appears just above the valence band edge localized on C-H bond that is followed by $1a''$ level, i.e., the descendant SiV related level. The $2a''$ level is localized mostly on the two carbon dangling bonds in the second vacancy. These states are occupied by three electrons in the neutral charge state. We found single and double acceptor levels at $E_V + 1.19$ eV and $E_V + 2.61$ eV, respectively (see Fig. 9). The neutral and $(2-)$ states have $S = 1/2$ spin and can be principally observed by EPR. The $(-)$ state is a nonparamagnetic singlet.

Indeed, the SiV_2:H(0) defect was assigned to the WAR3 EPR center in diamond based on combined experimental studies and DFT PBE simulations [17]. We list our calculated DFT PBE hyperfine parameters without core-polarization correction in order to have a direct comparison with the previous study [17] in Table IV. Again, the difference in the simulation results can be explained by the different treatment of the basis sets and the ion potentials. We also calculated the hyperfine parameters with HSE06 functional within our framework. The small hyperfine signal on the hydrogen nuclei is relatively well reproduced but the hyperfine signal on the ^{29}Si nuclei spin is overestimated. The spin polarization of the electron is dominated by the SiV related $1a''$ orbital, thus the same overestimation of ^{29}Si hyperfine constants occur as that for the SiV(0) defect.

We discuss here briefly the nature of these states from a theoretical point of view that affects the methodology to calculate the hyperfine parameters. The HSE06 functional may break the symmetry of the Kohn-Sham wave functions with respect to the space-group symmetry of the defective supercell, i.e., the Kohn-Sham wave functions are not necessarily the eigenstates of the corresponding space group of the defective supercell. We call these Kohn-Sham wave functions "symmetry-broken" wave functions in this context. We found that HSE06 total energy of the SiV_2:H(0) is about 0.18 eV deeper with symmetry-broken wave functions than that obtained by wave functions following the symmetry of the system. Löwdin called this effect "symmetry dilemma" in Hartree-Fock theory [55] that also applies to hybrid DFT due to the presence of the Fock operator [56]. However, the symmetry-broken solution leads to symmetry-broken spin density too which yields artificial hyperfine parameters. Hence, we always calculate the hyperfine parameters with such Kohn-Sham wave functions within the hybrid DFT approach that truly represent the space group of the defective supercell. However, the total energy of the system is calculated with symmetry-broken Kohn-Sham wave functions that enter the equation of formation energies or related quantities. The appearance of a symmetry-broken solution within HSE06 approach needs further discussion. In our particular system,

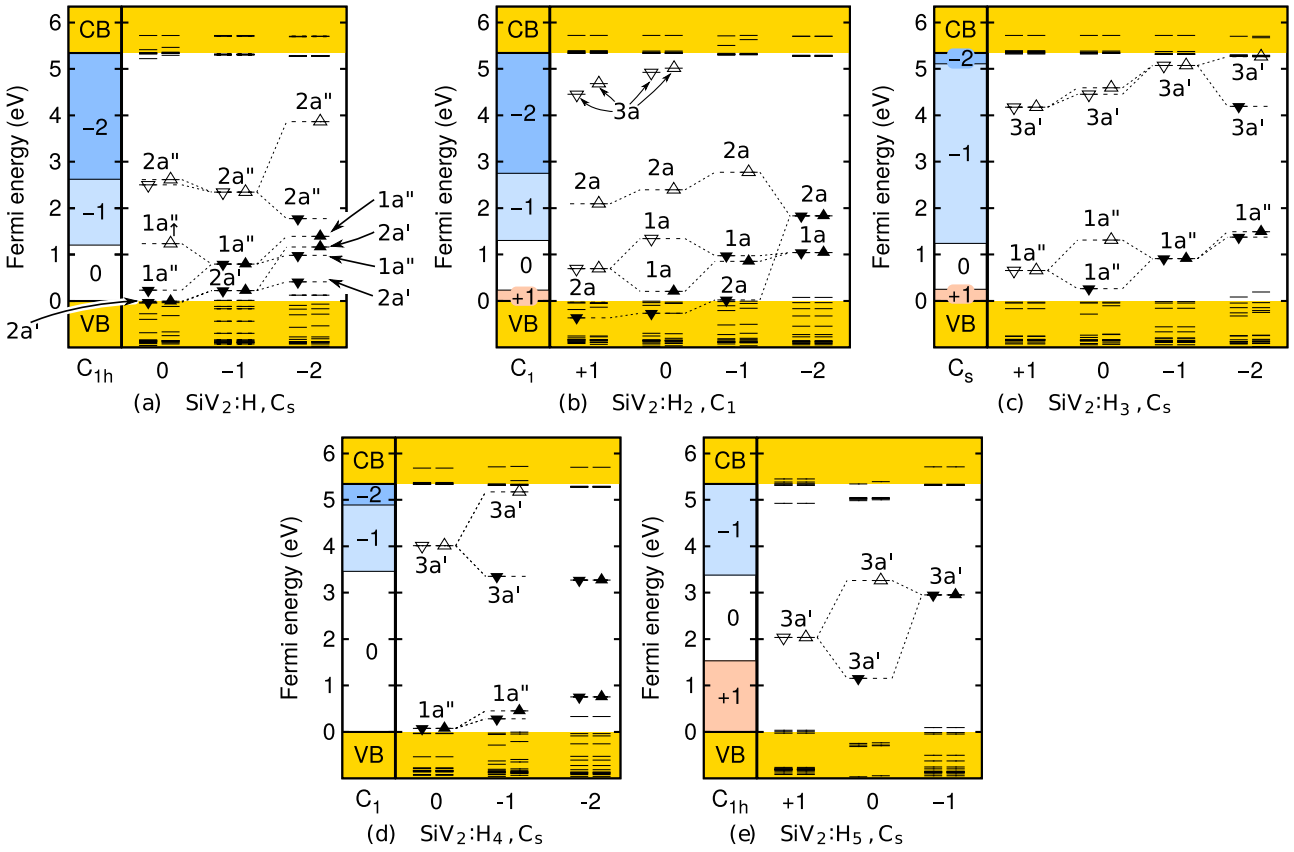

FIG. 9. (Color online) Charge transition levels and localized Kohn-Sham levels within the diamond gap. All results are obtained with HSE06 hybrid functional. The filled triangles represent occupied electrons whereas unfilled ones represent empty states. The spin-up and spin-down channels are shown separately, as symbolized with the orientation of the triangle. Due to spin-polarized calculations the spin-up and spin-down states may split in energy.

the second vacancy has two orbitals ($2a'$, $2a''$) localized in the different parts of the vacancy. In the symmetry-broken solution the character of these two states disappears but rather mixtures of these two states appear [57]. This is a sign of highly correlated orbitals (strong Coulomb interaction between localized electrons) where the exact solution of the many-body wave function would be a two-determinant open-shell singlet state in the Hartree-Fock picture. In Kohn-Sham DFT the single-particle Kohn-Sham wave functions are only used to express the many-body charge density of the system via the exchange-correlation functional, in order to obtain the total energy of the ground state. In practice it has been found for the case of hydrogen dissociation [58,59], various biradicals [58], complex systems [58], and model quantum dots [57,60,61] that *spin-polarized* hybrid DFT functionals are able to predict well the energy order of open-shell singlet and triplet states within the symmetry-broken approach: symmetry-broken spin-polarized hybrid DFT may cover most of the static correlation [62]. Vacancy related defects in diamond often fall to the category of highly correlated systems where HSE06 is still able to reproduce the experiment within about 0.2 eV accuracy as was partially discussed in our previous study (e.g., the N_2V defect in Ref. [44]).

TABLE IV. Experimental and theoretical hyperfine parameters for the neutral SiV_2:H defect. We provide the direction of hyperfine constants in parentheses in spherical coordinates (ϑ and φ angles, respectively). ϑ is the angle from [001] while φ is the angle from [100] in a (001) plane.

	Type	A_{xx} (MHz)	A_{yy} (MHz)	A_{zz} (MHz)
Expt.[a]	^{1}H	$\mp$2.9 (61,45)	$\pm$2.3 (151,45)	$\pm$0.4 (90,315)
	^{29}Si	$\pm$92 (43,45)	$\pm$96 (133,45)	$\pm$96 (90,315)
PBE[a]	^{1}H	-1 (27,45)	2 (117,45)	1 (90,315)
	^{29}Si	100 (53,45)	101 (143,45)	103 (90,315)
PBE	^{1}H	-1 (25,45)	0 (116,45)	1 (90,315)
	^{29}Si	60 (40,45)	62 (130,45)	61 (90,315)
HSE06	^{1}H	-2 (30,45)	3 (120,45)	0 (90,135)
	^{29}Si	125 (52,45)	122 (142,45)	127 (90,315)

[a]Reference [17].

We calculated the excitation energy of the system by promoting an electron from the $1a'$ level to the higher level in the neutral charge state. The vertical excitation and the zero-phonon line energies are 1.29 and 1.15 eV, respectively, resulting in 0.15-eV relaxation energy upon optical excitation. The calculated local vibration modes are at 3197 cm^{-1} (a' stretch mode) and 1740 cm^{-1} (a' bending mode). The last a'' bending mode is smeared into the diamond phonon band at 900 ± 100 cm^{-1}. The a' Si-related quasilocal mode along the [111] direction is at 326 cm^{-1}, and the other two modes are at 456 cm^{-1} a' and 466 cm^{-1} a'', respectively.

TABLE V. HSE06 hyperfine parameters of the SiV_2:H(2−) defect. The atom labels are shown in Fig. 11. We provide the direction of hyperfine constants in parentheses in spherical coordinates (ϑ and φ angles, respectively). ϑ is the angle from [001] while φ is the angle from [100] in a (001) plane.

Nuclei	A_{xx} (MHz)	A_{yy} (MHz)	A_{zz} (MHz)
$^{1}H_1$	6.7 (78,192)	−15 (47,113)	16 (135,90)
^{29}Si	24 (135,90)	25 (74,17)	31 (50,121)
$^{13}C_1$	159 (110,333)	159 (45,85)	290 (128,227)
$^{13}C_1'$	159 (115,23)	159 (45,85)	290 (125,311)
$^{13}C_2$	−11 (79,11)	−11 (135,90)	−13 (47,111)
$^{13}C_3$	−13 (44,5)	−15 (101,83)	−15 (49,163)
$^{13}C_3'$	−13 (87,227)	−15 (167,122)	−15 (77,317)
$^{13}C_4$	−10 (71,310)	−13 (151,258)	−13 (69,33)
$^{13}C_4'$	−10 (44,152)	−13 (118,96)	−13 (60,205)
$^{13}C_5$	16 (42,173)	17 (72,62)	25 (127,318)
$^{13}C_5'$	16 (85,312)	17 (33,35)	25 (123,225)
$^{13}C_6$	17 (91,45)	17 (33,134)	26 (123,315)
$^{13}C_6'$	17 (135,359)	17 (67,294)	26 (126,223)
$^{13}C_7$	20 (43,94)	20 (110,26)	30 (126,312)
$^{13}C_7'$	20 (47,94)	20 (115,338)	30 (127,228)

TABLE VI. HSE06 hyperfine parameters of the SiV_2:H_2(−) defect. The atom labels are shown in Fig. 11. We provide the direction of hyperfine constants in parentheses in spherical coordinates (ϑ and φ angles, respectively). ϑ is the angle from [001] while φ is the angle from [100] in a (001) plane.

Nuclei	A_{xx} (MHz)	A_{yy} (MHz)	A_{zz} (MHz)
$^{1}H_1$	−22 (133, −104)	−19 (82,174)	28 (44, −88)
$^{1}H_2$	−18 (132,25)	−17 (74,99)	−25 (47, −7)
^{29}Si	6 (23, −50)	5 (67,145)	7 (95, −128)
$^{13}C_1$	19 (96, −50)	18 (36,32)	32 (55, −136)
$^{13}C_1'$	19 (46,24)	18 (106, −49)	36 (48, −124)
$^{13}C_2$	−11 (79,11)	−11 (135,90)	−13 (47,111)
$^{13}C_3$	−13 (44,5)	−15 (101,83)	−15 (49,163)
$^{13}C_3'$	−13 (87,227)	−15 (167,122)	−15 (77,317)
$^{13}C_4$	−10 (71,310)	−13 (151,258)	−13 (69,33)
$^{13}C_4'$	−13 (44,152)	−15 (118,96)	−15 (60,205)
$^{13}C_5$	16 (42,173)	17 (72,62)	25 (127,318)
$^{13}C_5'$	16 (85,312)	17 (33,35)	25 (123,225)
$^{13}C_6$	20 (43,94)	20 (110,26)	30 (126,312)
$^{13}C_6'$	20 (47,94)	20 (115,338)	30 (127,228)
$^{13}C_7$	17 (91,45)	17 (33,134)	26 (123,315)
$^{13}C_7'$	17 (135,359)	17 (67,294)	26 (126,223)

We report results on the other charge states of SiV_2:H defect. In the negative charge state the two lowest energy defect states are occupied by four electrons resulting in a singlet ground state which is not observable by EPR. In the symmetrical wave-function approach, the $2a'$ and $1a'$ states are occupied and the $2a''$ state is empty. This ground-state many-body wave function has $^{1}A'$ symmetry. When an electron is promoted from the intermediate $1a'$ state to the $2a''$ then this excited state has $^{1}A''$ character. However, the character of these states disappears in the symmetry-broken hybrid DFT approach which makes here the excited-state calculation within the ΔSCF method ambiguous. Thus, we calculated the energy of the excited state within ΔSCF by the symmetrical wave-function approach that is calculated with respect to the total energy of the ground state as obtained by the same approach. Then we add the energy difference (0.11 eV) between those states as obtained by the symmetry-broken and symmetrical wave-function approaches for the ground-state electron configuration. The final vertical excitation and zero-phonon line energies are 1.40 and 1.26 eV, respectively. The calculated vibration modes are very similar to that obtained in the neutral charge state. The details about these defect wave functions and vibration modes will be explained in Sec. IV (see Figs. 12 and 13). Finally, we list the hyperfine signals of the defect in the doubly negative charge state in Table V that may be observed in nitrogen contaminated diamond.

F. Complex of SiV_2 defect with two hydrogen atoms: The SiV_2:H_2 defect

Two hydrogen atoms should saturate two dangling bonds in the SiV_2 defect. According to our calculations the most stable configuration has C_1 symmetry with both hydrogen bonds in the second vacancy which are labeled as position 4 and 5 in Fig. 1. This configuration is slightly more stable than the configuration with C_s symmetry by about 0.11 eV.

Two deep localized orbitals appear in the gap which are occupied by two electrons in the neutral charge state (see Fig. 9). The $1a$ state is originated from the SiV ancestor whereas the $2a$ state is originated from the carbon dangling bond in the second vacancy, similar to the case of the SiV_2:H defect. A third empty $3a$ state also appears very close to the conduction-band edge that is localized in the empty space of the vacancies near the Si atom but plays no role in the electrical or optical activity of this defect. We found that the open-shell singlet state is the ground state whereas the triplet state and a closed-shell singlet state follows this hierarchy by 0.13 and 0.29 eV, respectively. The neutral ground state is a singlet and not visible by EPR spectroscopy. As the occupied $2a$ state falls into the valence band the lowest energy zero-phonon optical transition at 1.13 eV results in such an excited state where the hole is partially delocalized on the valence-band edge, whereas it is at 1.28 eV when the hole is indeed localized on the $2a$ state in the excited state. The calculated H-related vibration modes are at 3316 cm^{-1}, 2949 cm^{-1} (stretch modes), and 1554 cm^{-1} (bending mode). The remaining bending modes are smeared into the diamond phonon bands at around 1300 and 1000 cm^{-1}. The Si related quasilocal vibration mode along the [111] direction is at 346 cm^{-1}, and the other two modes lie approximately at 466 and 475 cm^{-1}.

The calculated donor level is very close to the valence-band edge (see Fig. 9), thus the (+) charge state does not likely occur. The calculated acceptor levels are at $E_V + 1.27$ eV and $E_V + 2.90$ eV, respectively. The (−) state has $S = 1/2$ electron spin that may be detected by EPR. The calculated hyperfine parameters are listed in Table VI. We note that the hyperfine constants of ^{29}Si are predicted to be small because the SiV descendant $1a$ state is fully occupied hence it does not contribute to the spin density, in contrast to the case of SiV:H(0) or SiV:H_2(−) defects. Nevertheless, the two inequivalent ^{1}H hyperfine parameters are very characteristic due to the low

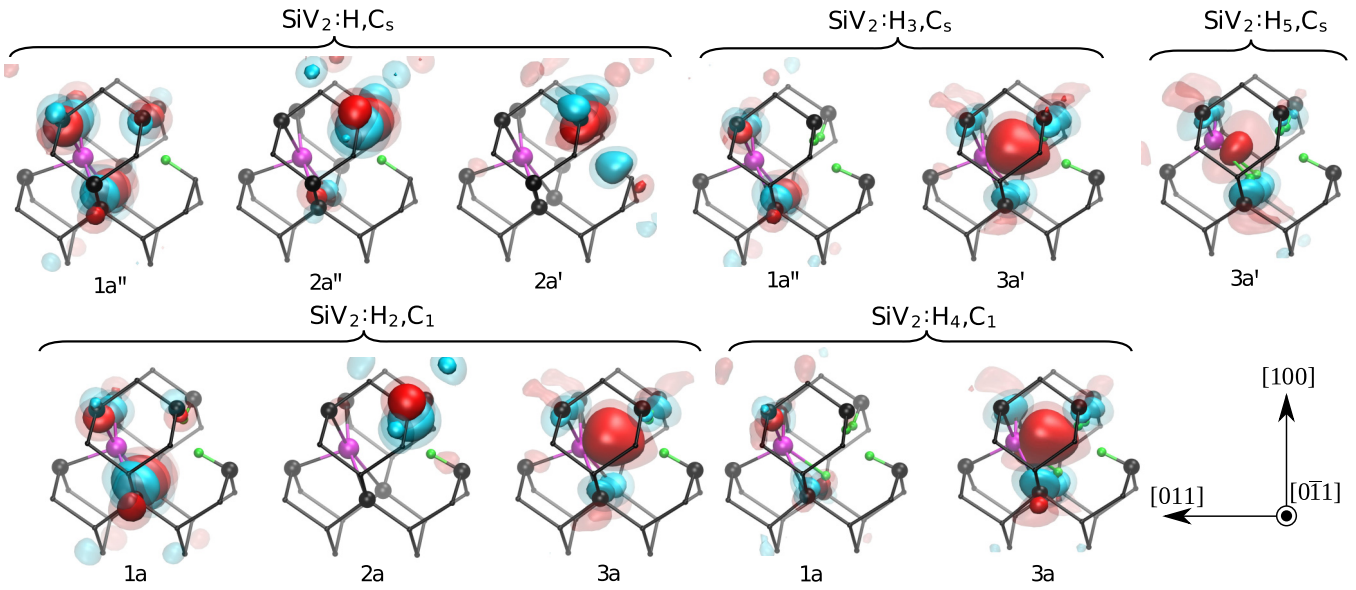

FIG. 10. (Color online) The defect wave functions of the SiV_2:H_n defects. All states are shown for the down-spin component in the neutral charge state of the systems except for the SiV_2:H where the negatively charged state is shown. The solid red and blue lobes represent the wave function with an isovalue of ± 0.025 while the transparent ones represent the isosurface of ± 0.015.

symmetry of the defect. The calculated ZPL energy is 1.28 eV. In the $(2-)$ state all the deep defect levels in the gap are occupied forming a closed-shell singlet.

G. Complex of SiV_2 defect with three hydrogen atoms: The SiV_2:H_3 defect

The three hydrogen atoms saturate the three dangling bonds in the second vacancy of the SiV_2:H_3 complex (see Fig. 10). Two levels appear in the gap that originate from an asymmetric $1a''$ state and a symmetric $3a'$ state in this order. In the neutral charge state these states are occupied by a single electron forming the $S = 1/2$ spin state. The calculated hyperfine signals are listed in Table VII. As the $2a$ state falls into the valence band the lowest energy zero-phonon optical transition at 1.11 eV results in such an excited state where the hole is partially delocalized on the valence-band edge, whereas it is at 1.10 eV when the hole is indeed localized on the $2a$ state in the excited state. The hydrogen related stretch vibration modes are at 3638 cm^{-1} (a'), 3460 cm^{-1} (a'), and 3389 cm^{-1} (a''). The bending modes are at 1459 cm^{-1} (a''), 1453 cm^{-1} (a'), and 1405 cm^{-1} (a'). The remaining two a'' and one a' bending modes fall into the phonon bands at around 950 ± 50 cm $^{-1}$. The Si related quasilocal modes are at 334 cm^{-1} (a' along roughly the [111] direction), 467 cm^{-1} (a''), and 480 cm^{-1} (a') where the latter two vibrate perpendicular to the [111] direction.

The defect is principally stable in $(+)$, (0), $(-)$, and $(2-)$ charge states, nevertheless the calculated $(+|0)$ and $(-|2-)$ levels are too close to the valence- and conduction-band edges, respectively, thus they do not likely occur in diamond. The calculated $(0|-)$ acceptor level is at $E_V + 1.24$ eV. In the $(-)$ charge state the $1a''$ state is fully occupied whereas the $3a'$ state is empty forming a closed-shell singlet state.

H. Complexes of SiV_2 defect with four and five hydrogen atoms: The SiV_2:H_4 and SiV_2:H_5 defects

Three hydrogen atoms completely saturate the dangling bonds of the second vacancy in the SiV_2 defect. The fourth and fifth hydrogen atoms form C-H bonds in the first vacancy of the defect near the Si atom. In the SiV_2:H_4 complex two defect levels appear: the first one is originated from the $1a$ state and the second one from the $3a$ state, similar to the case of SiV_2:H_3. Two electrons occupy these states in the neutral charge state forming a closed-shell singlet ground state. The $(0|-)$ level lies relatively high in the gap at around $E_V + 3.5$ eV whereas the $(-|2-)$ level is at around $E_V + 4.9$ eV. We note that the geometry significantly changes when the $(-)$ state is further ionized.

TABLE VII. HSE06 hyperfine parameters of the SiV_2:$H_3(0)$ defect. The atom labels are shown in Fig. 11. We provide the direction of hyperfine constants in parentheses in spherical coordinates (ϑ and φ angles, respectively). The first value describes the angle about the [001] direction while the second one is the angle from [100] for the projection into the (001) plane.

Nuclei	A_{xx} (MHz)	A_{yy} (MHz)	A_{zz} (MHz)
$^{1}H_1$	−3 (30,45)	0 (90, −45)	4 (60, −135)
$^{1}H_2$	4 (92, −60)	3 (60,29)	8 (30, −147)
$^{1}H_2'$	4 (88, −30)	3 (60,61)	8 (30, −123)
^{29}Si	118 (90,135)	114 (29, −135)	122 (119, −135)
$^{13}C_1$	23 (52,14)	23 (54, −110)	55 (58,133)
$^{13}C_1'$	23 (52,76)	23 (126,20)	55 (58, −43)
$^{13}C_2$	71 (73,56)	70 (37,169)	157 (58, −45)
$^{13}C_2'$	71 (73,34)	70 (143,101)	157 (58,135)
$^{13}C_3$	−9 (68,75)	−7 (60, −29)	−10 (39, −165)
$^{13}C_3'$	−9 (112, −165)	−7 (60,119)	−10 (39, −105)
$^{13}C_4$	8 (55, −170)	8 (56,71)	17 (54, −49)
$^{13}C_4'$	8 (55, −100)	8 (124, −161)	17 (54,139)
$^{13}C_5$	6 (64,68)	6 (46, −175)	13 (55, −42)
$^{13}C_5'$	6 (64,22)	6 (134,85)	13 (55,132)
$^{13}C_6$	8 (27,145)	7 (86,47)	17 (63, −45)
$^{13}C_6'$	8 (153,125)	7 (86,43)	17 (63,135)

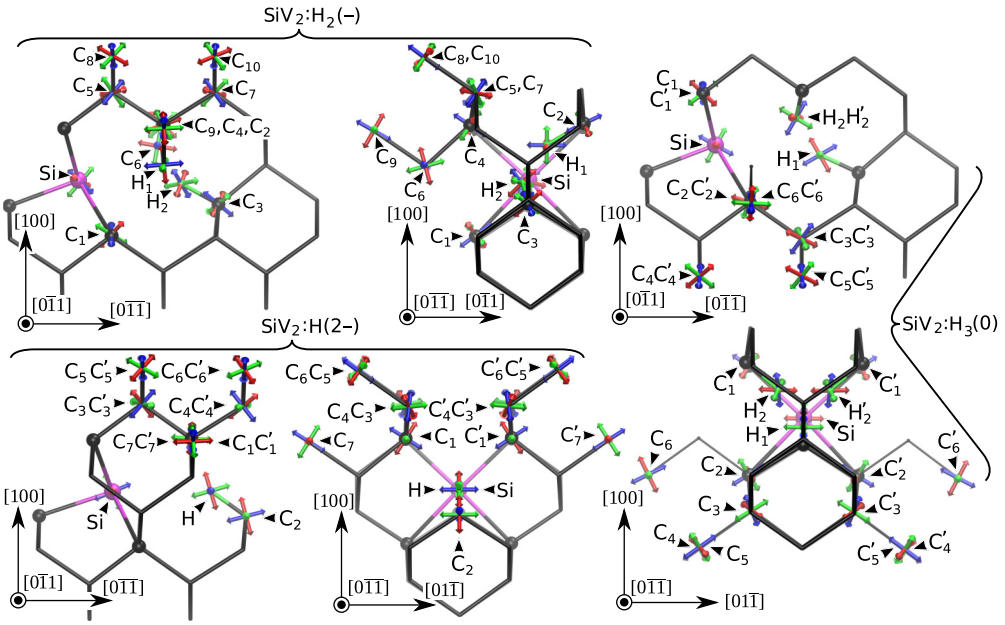

FIG. 11. (Color online) The direction cosine of ^{1}H, ^{13}C, and ^{29}Si hyperfine constants for the SiV_2:$H_2(-)$, SiV_2:H(2−), and SiV_2:$H_3(0)$ complexes. The hyperfine constants can be found in Tables VI, V, and VII, respectively. The red, green, and blue arrows represent the direction cosine of the hyperfine constants A_{xx}, A_{yy}, and A_{zz}, respectively.

In the SiV_2:H_5 defect no unterminated dangling bond remains in the complex. As a consequence, only the C-H related antibonding state appears in the gap. This $3a'$ state is occupied by a single electron in the neutral charged state. This defect can exist in (+) and (−) charge states with a singlet ground state.

IV. ORIGIN OF THE 1.018-EV ABSORPTION CENTER AND ITS POTENTIAL FOR QUANTUM MEMORY APPLICATION

The 1.018-eV absorption center was measured at 4 K in silicon contaminated diamond sample (see Fig. 12) where the multiple phonon replica is visible with equidistant energy with respect to the ZPL peak with energy of about 0.042 eV that corresponds to 338.7 cm^{-1} [14]. The silicon contaminated diamond sample was annealed at 2000 °C in this experiment. At all conditions the SiV(0) and SiV(−) ZPL signals were visible but the intensity of SiV(0) ZPL signal decreased with respect to the SiV(−) ZPL signal when the annealing temperature was increased from 1000 to 2000 °C. We note that the KUL3 SiV:H(0) EPR signal anneals out at 1200 °C whereas the WAR3 SiV_2:H(0) EPR signal disappears at 1600 °C annealing. From these experimental facts one cannot disregard that a 1.018-eV center may appear at >1600 °C annealing too. Since both SiV(0) and SiV(−) centers are detected in the sample, thus we assume that the Fermi level should be around $E_V + 1.4$ eV where the defect changes its charge state from (0) to (−). The increased concentration of SiV(−) over SiV(0) at elevated annealing temperatures indicate that the position of the Fermi level shifts upward in this procedure.

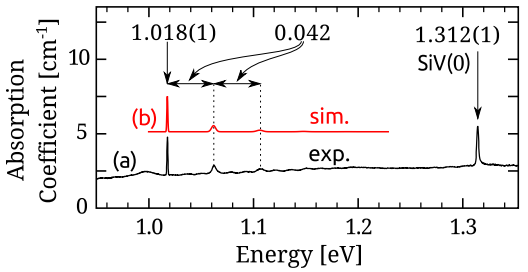

FIG. 12. (Color online) Panel (a) shows the experimental data (exp.) taken from Ref. [14]. The SiV defect is visible in both neutral (1.31 eV) and negatively charged (1.68 eV) states after annealing at 2000 °C. The 1.68-eV line is not shown in the figure. The red inset (b) shows a simulated spectrum (sim.) of the SiV_2:H(−) defect. The ZPL position of the simulation was aligned to the experimental ZPL peak for the sake of clear comparison of the absorption line shapes. The area under the peaks are calculated from $S = 0.72$ [Eq. (A6)] and the linewidths are taken from the experimental spectrum (a) with Gaussian fits. The extracted full width at half maximum values from the experimental data are 0.9, 4.0, 5.8, 7.2 meV for ZPL, first, second, and third replica peaks, respectively.

The experimental conditions strongly suggest that the 1.018-eV center is related to Si impurity. Excluding SiV:H(0) and SiV_2:H(0) defects, SiV_2, SiV_2:H(−), SiV_2:$H_2(0)$, SiV_2:$H_3(0)$ complexes yield ZPL energies of about 1.0 ± 0.2 eV and Si-related vibration mode at around 0.042 ± 0.004 eV. Relative large uncertainty in the calculated ZPL and vibration modes is considered because of the presence of highly correlated states in some of these defects, and even 512-atom supercell calculation does not suffice fully convergent results on the quasilocal vibration modes. We discuss these defects as candidates for the origin of the 1.018-eV absorption center.

The SiV_2 defect has multiple empty states both in its neutral and single negative charge states implying absorption both in the infrared and visible (see Fig. 8). However, such behavior was not reported for this center, thus the SiV_2 defect unlikely accounts for the 1.018-eV center. Both in SiV_2:$H_2(0)$

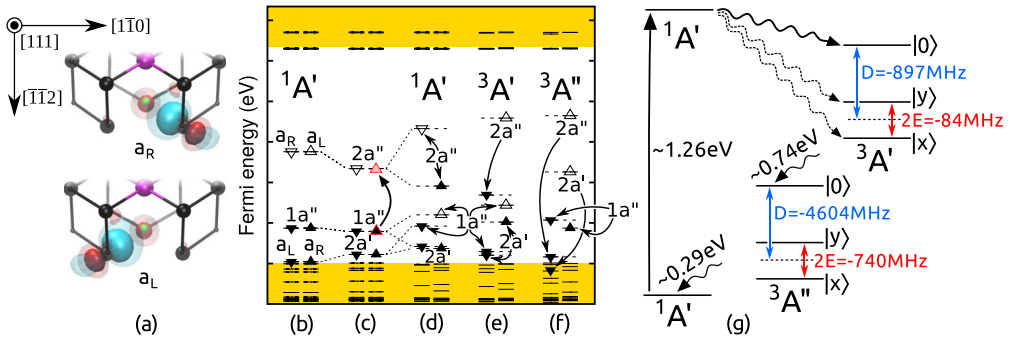

FIG. 13. (Color online) The calculated states of SiV_2:H(−) defect associated with the 1.018-eV absorption center and its proposed coherent manipulation of its electron-spin state by optical excitation. We show here the calculated energies that may have uncertainty of about 0.2 eV due to the limitation of the applied methodology to address multideterminant states. For details about the visualization of the Kohn-Sham levels and the wave functions, see Figs. 9 and 10, respectively. Panel (a) shows the symmetry-broken solution of the ground state with the symmetry-broken a_L and a_R orbitals. The corresponding Kohn-Sham levels are shown in (b) forming the many-body ground state $^1A'$ in (g). The electron configuration of the symmetric wave-function approach in (c) results in a higher total energy by 0.11 eV where the inclined up-arrow represents the promotion of the electron in the ΔSCF process resulting in the excited-state electron configuration in (d) that forms $^1A'$ excited state in (g). The high-spin electron configuration in (e) gives rise to the short-living $^3A'$ state in (g). The high-spin electron configuration in (f) appears as the metastable $^3A''$ state in (g). The D and E parameters of the zero-field splitting of the high spin states are depicted (not scaled for the sake of the clarity). The thick (thin) wavy arrows represent strong (weak) spin-orbit mediated nonradiative decay from the $^1A'$ to the $^3A'$ state. The electron may decay either radiatively or nonradiatively but spin-conserving between the triplet states. Finally, nonradiative decay occurs mediated by spin-orbit interaction between the $^3A''$ metastable state and $^1A'$ ground state.

and SiV_2:H_3(0) complexes the excitation from VBM has lower energy than that from a localized state, although these two energies agree within the numerical accuracy of the calculations for SiV_2:H_3(0). In the experimental spectrum the ZPL peak is sharp and it does not imply transition from a delocalized band. SiV_2:H_3(0) cannot be fully excluded based on this ground. Nevertheless, this defect is paramagnetic with possessing $S = 1/2$ electron spin with characteristic ^{29}Si and ^{1}H hyperfine signals but no such EPR center was reported in the experiments [14]. On the other hand, the pseudodynamic Jahn-Teller effect may occur in this system that can shorten the coherence time of the electron spin and suppress its EPR signal. These defects have (0|−) acceptor level at around $E_V + 1.3$ eV, thus the negative charge states should also appear in the diamond sample at elevated temperature annealing. These defects have larger ZPL energies than ∼1.0 eV in their (−) charge states that can be estimated from their charge transition levels (see Fig. 3). In summary, SiV_2:H_2 and SiV_2:H_3 defects are not the likely candidates for the 1.018-eV absorption center.

Finally, we discuss the SiV_2:H(−) defect. Its neutral counterpart, the WAR3 EPR center, anneals out at 1600 °C. The calculated (0|−) acceptor level of the defect is at $E_V + 1.19$ eV. As the position of the Fermi level shifts up at very high-temperature annealing of the diamond (at around $E_V + 1.4$ eV and above) the concentration of the neutral charge state at 1600 °C may decrease substantially but the concentration of the negative charge state can increase which can become clearly visible in optical absorption by 2000 C° annealing. We note that no careful experiment has been carried out to correlate the WAR3 EPR signal and the 1.018-eV absorption center, thus our proposed scenario is reasonable and can be later verified in future experiments. The calculated Si-related vibration mode vibrating along the [111] direction is at 343 cm^{-1}. We calculated the participation of this vibration mode in the absorption spectrum (see the Appendix for the methodology). According to our calculations the Si atom moves 0.051 Å along the [111] direction upon optical excitation. The effective mass of this vibration mode is 49 a.u. derived from the effective spring constant that results in $S = 0.74$, i.e., the Huang-Rhys factor [63] of this vibration. This parameter defines the relative intensities between ZPL and vibration replica peaks. Finally, the simulated line shape can be directly compared to the experimental plot in Fig. 12. The agreement is excellent. Our methodology also explains why the H-related vibration peaks are not visible in the absorption spectrum. For the optically allowed a' H-related vibration modes the H atom moves a maximum of 0.028 Å upon optical excitation and the characteristic length scale of the vibrations is about 0.15 Å. As a consequence, its $S < 0.004$ holds, thus the intensity of its first vibration replica is much less than 1% compared to the intensity of the ZPL peak which is hardly visible in the spectrum. Thus, the SiV_2:H(−) defect is the best candidate for the 1.018-eV absorption center among the considered Si-related defects. The vibration mode shifts downward successively by 3.1 cm^{-1} when ^{28}Si is replaced by ^{29}Si that is again replaced by ^{30}Si. Thus, optical measurement may directly identify the chemical composition of the 1.018-eV absorption center. We further discuss the SiV_2:H(−) defect. When the defect is photoexcited with energy close to ZPL then the defect may emit light at around 1.018 eV at low temperatures. This emission occurs between two $^1A'$ singlet states. According to our calculations shelving triplet states appear between these singlet states [see Fig. 13(g)]. Due to the low symmetry the spin levels will definitely split due to the electron-spin–electron-spin interaction in the absence of external magnetic field where the corresponding zero-field splitting parameters can be found in Fig. 13). With assuming different scattering rates between the ES $^1A'$ state and the $m_S = 0$ and $m_S = \pm 1$ spin states of the short-living $^3A'$ one can optically populate the $m_S = 0$ of the metastable $^3A''$

triplet by optical excitation. The different spin-orbit scattering rate may occur between the proposed states because the spin-orbit interaction should connect the same type of carbon dangling-bond orbitals without changing its character in this process which is more likely with an $l_z s_z$ type of operator than with an $l_{\pm} s_{\mp}$ type of operator because the latter would change the character of the orbital. The character of the electron and hole orbitals are the same for the corresponding ES $^1A'$ and $^3A'$ states. In the metastable $^3A''$ state the calculated hyperfine constants are ($A_{xx} = -3.4$ MHz, $A_{yy} = 19.2$ MHz, $A_{zz} = -20.3$ MHz) for ^{1}H and ($A_{xx} = 3.1$ MHz, $A_{yy} = 1.4$ MHz, $A_{zz} = 3.6$ MHz) for ^{29}Si, respectively. The electron-spin information in the $^3A''$ state may be stored by the ^{29}Si nuclear spin mediated by the hyperfine interaction, similarly to the process demonstrated in the ST1 center of diamond [64]. We finally propose that the photoexcitation of the 1.018-eV center should be reinvestigated in detail whether optically detected magnetic resonance may be associated with this defect that can be an alternative to realize a long-living [64] quantum memory in diamond.

V. CONCLUSION AND SUMMARY

We systematically studied complexes of silicon, vacancy, and hydrogen atoms in diamond by means of *ab initio* plane-wave supercell calculations. We listed their parameters that might be observed in magnetic, optical, or vibration spectroscopies. One of the motivations of this study was to characterize and identify Si-related defects that might explain the "hidden" silicon [14,15] in diamond. By assuming the incorporation of silane (SiH_4) and related silicon-hydrogen radicals into diamond as building blocks during CVD growth, complexes of silicon and hydrogen atoms may occur in diamond. Among the considered defects we found that SiV:H_2 and SiV_2:H_4 defects are basically electrically inactive defects, and they have optical transition only in the farther ultraviolet region. These defects may be detected via their characteristic C-H vibration bands by infrared absorption or Raman-scattering spectrum. These defects might partially account for Si-related but optically invisible defects in diamond. In addition, we tentatively assign the 1.018-eV absorption center to the negatively charged SiV_2:H(−) defect in diamond. We find that this defect is a suitable candidate for further optical studies toward the realization of an alternative long-living solid-state quantum memory.

ACKNOWLEDGMENTS

A.G. acknowledges the support from NIIF Supercomputer Center Grant No. 1090, EU FP7 Grant No. 611143 (DIADEMS), and the Lendület program of the Hungarian Academy of Sciences.

APPENDIX: *AB INITIO* CALCULATION OF THE INTENSITY OF THE PHONON REPLICA ASSOCIATED WITH QUASILOCAL VIBRATION MODES IN THE PHOTOEXCITATION SPECTRUM

Here we describe a simplified approach to calculate the photoexcitation spectrum at the *ab initio* level when the phonon sideband is dominated by (quasi)local vibration modes. Our methodology can be applied upon the following conditions:

(i) the optical transition can be described by Franck-Condon principle [65];

(ii) the potential-energy surface of the electronic ground (GS) and excited (ES) states is approximately the same and they are harmonic;

(iii) the relaxation energy of the system upon optical excitation is relatively small, i.e., the so-called Huang-Rhys factor [63] is less than or equal to 1;

(iv) the motion of the nuclei upon optical excitation is predominantly connected to the normal coordinate of a *single* (quasi)local vibration mode.

The Franck-Condon principle applies to many polyatomic systems and may break down for Jahn-Teller systems with degenerate many-electron states. In the case of SiV:H_x and SiV_2:H_y defects, the symmetry is low which implies that the Franck-Condon principle is valid, thus the relative intensities between the zero-phonon line (ZPL) and the phonon replica should be related to

$$|\langle \Phi_{\mathrm{GS}} | \Phi_{\mathrm{ES}} \rangle|^2, \tag{A1}$$

where Φ is the many-body vibration function in the corresponding GS and ES. Since Φ contains $3N-3$ coordinates (where N is the number of atoms in the supercell), the calculation of this overlap becomes onerous when these coordinates are different in GS and ES. In our special polyatomic systems the nature of the electronic GS and ES is very similar, thus it is good approximation to assume an almost equal potential-energy surface (PES) in GS and ES. In the harmonic approximation of PES the many-body Φ is the product of $H_{\mathrm{n}}(x_i)$ nth Hermite polynomials multiplied by an exponential function,

$$\psi_n(x_i) = \frac{1}{\sqrt{2^n n!}} \pi^{-1/4} e^{-x_i^2/2} \mathrm{H}_n(x_i), \tag{A2}$$

where x_i is the reduced or dimensionless coordinate of the one-dimensional quantum harmonic oscillator with a vibration quantum n, and i runs from 1 to $3N-3$. As the measurement temperature was low in our special case (1.018-eV absorption center in diamond) the anharmonic effects may be indeed small. In the case of the SiV:H_x and SiV_2:H_y defect the relaxation energy upon optical excitation fall typically in the 0.1–0.25-eV region that is relatively small. We note that the convergent calculation of the Huang-Rhys factor of the full system from first principles is a relatively notorious procedure [66] which is a key step to calculate the absorption or luminescence line shapes associated with phonons. Here we introduce rather a simplification. In our example, the 1.018-eV absorption center shows a relatively sharp ZPL and some small bumps equidistant from the ZPL line and from each other in the spectrum (see Fig. 12) that are associated with the phonon replica. This is a clear indication that the Huang-Rhys factor of this system should be in the region of 0.1–1.0, thus we can indeed assume that a quasilocal vibration mode is coupled strongly in the optical excitation. We particularly found that the Si atom moves along the [111] direction upon optical excitation of these defects (see Fig. 1). We could clearly identify such a single quasilocal vibration mode in our 512-atom supercell calculation where the Si atom moves along this direction. Thus,

we can assume that this single vibration mode predominantly couples to the optical transition. This single vibration mode is a displaced oscillator in the electronic excited state where half of the displacement in dimensionless unit d may be calculated as $d = \Delta X/(2x_0)$ where ΔX is the real displacement of the Si atom in Å unit from GS to ES, and x_0 is the length scale of the corresponding oscillator in the same unit. The length scale of the oscillator can be determined by

$$x_0 = \sqrt{\frac{\hbar}{m^*\omega}}, \tag{A3}$$

where m^* is the reduced mass of the vibration with vibration frequency ω. The reduced mass can be derived as $m^* = \frac{k^*}{\omega^2}$ where k^* is the effective spring constant of the vibration. The value of ω with the corresponding eigenvector (normal coordinate) can be directly calculated with the *ab initio* code. The effective spring constant, in our special case, can be deduced from the 3×3 *ab initio* Hessian matrix of the Si atom where the value along the [111] direction should be taken.

By using the orthonormal property of the $\psi(x_i)$ functions, this approximation simplifies the problem of calculating the overlap between the vibration functions to

$$\begin{aligned}\langle\Phi_{GS}|\Phi_{ES}\rangle &= \int dx\psi_m(x)\psi_n(x-2d) = \int dx\psi_m(x+d)\psi_n(x-d)\\ &= \frac{1}{\sqrt{2^{n+m}n!m!}}\pi^{-1/2}e^{-d^2}\int dx e^{-x^2}\mathrm{H}_m(x-d)\mathrm{H}_n(x+d),\end{aligned} \tag{A4}$$

where m (n) is the vibration quantum number in GS (ES). Since e^{-d^2} is constant it does not influence the relative intensities hence it is dropped. The final integral can be analytically solved where the overlap (A) from GS to ES can be calculated as

$$A(m \to n) \sim \sum_{k=0}^{k\leqslant n,m}\binom{n}{k}\binom{m}{k}(2d)^{n+m-2k}2^{k-(n+m)/2} \times \frac{k!}{\sqrt{n!m!}}(-1)^k. \tag{A5}$$

The occupation of the vibration states depends on the temperature. In absorption measurements the process starts from GS. At the low-temperature limit only the ground state vibration function is occupied at the zero-point energy of the system. Indeed, this occurs for the 1.018-eV center where the absorption spectrum was recorded at 4 K. In that case $m = 0$ should be only considered in Eq. (A5). By introducing the $S \cong 2d^2$ dimensionless quantity (Huang-Rhys factor [63,67]) the intensity of absorption with the frequency Ω of the absorbed photons results in

$$I_n \sim \Omega|A(0 \to n)|^2 = (\omega_{ZPL} + n\omega)\frac{S^n}{n!}, \tag{A6}$$

where ω_{ZPL} is the ZPL energy. We use Eq. (A6) to calculate the relative intensities of the ZPL and phonon replica in the absorption spectrum. The linewidth of the ZPL and replica peaks depends on the lifetime and other broadening effects that is beyond the scope of our study. In the simulation of the absorption spectrum the broadening for a given peak is taken from the experimental spectrum.

[1] A. Zaitsev, V. Vavilov, and A. Gippius, Sov. Phys. Lebedev Inst. Rep. **10**, 15 (1981).

[2] C. M. Breeding and W. Wang, Diamond Relat. Mater. **17**, 1335 (2008).

[3] S. Amari, R. S. Lewis, and E. Anders, Geochim. Cosmochim. Acta **58**, 459 (1994).

[4] I. I. Vlasov, A. A. Shiryaev, T. Rendler, S. Steinert, S.-Y. Lee, D. Antonov, M. Vörös, F. Jelezko, A. V. Fisenko, L. F. Semjonova, J. Biskupek, U. Kaiser, O. I. Lebedev, I. Sildos, P. R. Hemmer, V. I. Konov, A. Gali, and J. Wrachtrup, Nat. Nanotechnol. **9**, 54 (2014).

[5] T. Müller, C. Hepp, B. Pingault, E. Neu, S. Gsell, M. Schreck, H. Sternschulte, D. Steinmüller-Nethl, C. Becher, and M. Atatüre, Nat. Commun. **5**, 3328 (2014).

[6] L. J. Rogers, K. D. Jahnke, M. H. Metsch, A. Sipahigil, J. M. Binder, T. Teraji, H. Sumiya, J. Isoya, M. D. Lukin, P. Hemmer, and F. Jelezko, Phys. Rev. Lett. **113**, 263602 (2014).

[7] J. P. Goss, R. Jones, S. J. Breuer, P. R. Briddon, and S. Öberg, Phys. Rev. Lett. **77**, 3041 (1996).

[8] J. P. Goss, P. R. Briddon, M. J. Rayson, S. J. Sque, and R. Jones, Phys. Rev. B **72**, 035214 (2005).

[9] C. D. Clark, H. Kanda, I. Kiflawi, and G. Sittas, Phys. Rev. B **51**, 16681 (1995).

[10] A. Gali and J. R. Maze, Phys. Rev. B **88**, 235205 (2013).

[11] C. Hepp, T. Müller, V. Waselowski, J. N. Becker, B. Pingault, H. Sternschulte, D. Steinmüller-Nethl, A. Gali, J. R. Maze, M. Atatüre, and C. Becher, Phys. Rev. Lett. **112**, 036405 (2014).

[12] L. J. Rogers, K. D. Jahnke, M. W. Doherty, A. Dietrich, L. P. McGuinness, C. Müller, T. Teraji, H. Sumiya, J. Isoya, N. B. Manson, and F. Jelezko, Phys. Rev. B **89**, 235101 (2014).

[13] U. F. S. D'Haenens-Johansson, A. M. Edmonds, B. L. Green, M. E. Newton, G. Davies, P. M. Martineau, R. U. A. Khan, and D. J. Twitchen, Phys. Rev. B **84**, 245208 (2011).

[14] U. F. S. D'Haenens-Johansson, Ph.D. thesis, University of Warwick, 2011.

[15] A. M. Edmonds, M. E. Newton, P. M. Martineau, D. J. Twitchen, and S. D. Williams, Phys. Rev. B **77**, 245205 (2008).

[16] J. P. Goss, P. R. Briddon, and M. J. Shaw, Phys. Rev. B **76**, 075204 (2007).

[17] U. F. S. D'Haenens-Johansson, A. M. Edmonds, M. E. Newton, J. P. Goss, P. R. Briddon, J. M. Baker, P. M. Martineau, R. U. A. Khan, D. J. Twitchen, and S. D. Williams, Phys. Rev. B **82**, 155205 (2010).

[18] J. P. Goss, R. Jones, M. I. Heggie, C. P. Ewels, P. R. Briddon, and S. Öberg, Phys. Rev. B **65**, 115207 (2002).

[19] T. Miyazaki, H. Okushi, and T. Uda, Phys. Rev. Lett. **88**, 066402 (2002).

[20] J. Goss, C. Ewels, P. Briddon, and E. Fritsch, Diamond Relat. Mater. **20**, 896 (2011).

[21] A. Stacey, T. J. Karle, L. P. McGuinness, B. C. Gibson, K. Ganesan, S. Tomljenovic-Hanic, A. D. Greentree, A. Hoffman, R. G. Beausoleil, and S. Prawer, Appl. Phys. Lett. **100**, 071902 (2012).

[22] J. Chevallier, F. Jomard, Z. Teukam, S. Koizumi, H. Kanda, Y. Sato, A. Deneuville, and M. Bernard, Diamond Relat. Mater. **11**, 1566 (2002).
[23] C. Glover, M. E. Newton, P. M. Martineau, S. Quinn, and D. J. Twitchen, Phys. Rev. Lett. **92**, 135502 (2004).
[24] M. J. Shaw, P. R. Briddon, J. P. Goss, M. J. Rayson, A. Kerridge, A. H. Harker, and A. M. Stoneham, Phys. Rev. Lett. **95**, 105502 (2005).
[25] K. Iakoubovskii, A. Stesmans, K. Suzuki, A. Sawabe, and T. Yamada, Phys. Rev. B **66**, 113203 (2002).
[26] J. P. Goss, P. R. Briddon, V. Hill, R. Jones, and M. J. Rayson, J. Phys.: Condens. Matter **26**, 145801 (2014).
[27] K. Iakoubovskii, A. Stesmans, K. Suzuki, J. Kuwabara, and A. Sawabe, Diamond Relat. Mater. **12**, 511 (2003).
[28] T. Kim, H. Kang, N. Park, Y. Son, J. Jeong, J. Woo, H. Choe, and C. Whang, J. Korean Phys. Soc. **37**, 304 (2000).
[29] E. Borchi, M. Bruzzi, C. Leroy, and S. Sciortino, J. Phys. D **31**, 609 (1998).
[30] E. Gheeraert, A. Deneuville, P. Gonon, M. Benabdesselam, and P. Iacconi, Phys. Status Solidi A **172**, 183 (1999).
[31] G. Kresse and J. Hafner, Phys. Rev. B **49**, 14251 (1994).
[32] G. Kresse and J. Furthmüller, Phys. Rev. B **54**, 11169 (1996).
[33] P. E. Blöchl, Phys. Rev. B **50**, 17953 (1994).
[34] J. P. Perdew, K. Burke, and M. Ernzerhof, Phys. Rev. Lett. **77**, 3865 (1996).
[35] T. A. Ivanova and B. N. Mavrin, Phys. Solid State **55**, 160 (2013).
[36] S. Baroni, S. de Gironcoli, A. Dal Corso, and P. Giannozzi, Rev. Mod. Phys. **73**, 515 (2001).
[37] R. J. Nemanich and S. A. Solin, Phys. Rev. B **20**, 392 (1979).
[38] J. Canisius and J. L. van Hemmen, J. Phys. C **18**, 4873 (1985).
[39] V. Ivády, T. Simon, J. R. Maze, I. A. Abrikosov, and A. Gali, Phys. Rev. B **90**, 235205 (2014).
[40] J. Heyd, G. E. Scuseria, and M. Ernzerhof, J. Chem. Phys. **118**, 8207 (2003).
[41] A. V. Krukau, O. A. Vydrov, A. F. Izmaylov, and G. E. Scuseria, J. Chem. Phys. **125**, 224106 (2006).
[42] A. Gali, E. Janzén, P. Deák, G. Kresse, and E. Kaxiras, Phys. Rev. Lett. **103**, 186404 (2009).
[43] P. Deák, B. Aradi, T. Frauenheim, E. Janzén, and A. Gali, Phys. Rev. B **81**, 153203 (2010).
[44] P. Deák, B. Aradi, M. Kaviani, T. Frauenheim, and A. Gali, Phys. Rev. B **89**, 075203 (2014).
[45] O. V. Yazyev, I. Tavernelli, L. Helm, and U. Röthlisberger, Phys. Rev. B **71**, 115110 (2005).
[46] K. Szász, T. Hornos, M. Marsman, and A. Gali, Phys. Rev. B **88**, 075202 (2013).
[47] S. B. Zhang and J. E. Northrup, Phys. Rev. Lett. **67**, 2339 (1991).
[48] G. Makov and M. C. Payne, Phys. Rev. B **51**, 4014 (1995).
[49] S. Lany and A. Zunger, Phys. Rev. B **78**, 235104 (2008).
[50] C. Freysoldt, J. Neugebauer, and C. G. Van de Walle, Phys. Rev. Lett. **102**, 016402 (2009).
[51] X. T. Trinh, K. Szász, T. Hornos, K. Kawahara, J. Suda, T. Kimoto, A. Gali, E. Janzén, and N. T. Son, Phys. Rev. B **88**, 235209 (2013).
[52] L. S. Bartell and B. L. Carroll, J. Chem. Phys. **42**, 1135 (1965).
[53] L. B. Handy, P. M. Treichel, L. F. Dahl, and R. G. Hayter, J. Am. Chem. Soc. **88**, 366 (1966).
[54] A. Janotti and C. G. Van de Walle, Nat. Mater. **6**, 44 (2006).
[55] P. Lykos and G. W. Pratt, Rev. Mod. Phys. **35**, 496 (1963).
[56] C. D. Sherrill, M. S. Lee, and M. Head-Gordon, Chem. Phys. Lett. **302**, 425 (1999).
[57] A. Harju, E. Räsänen, H. Saarikoski, M. J. Puska, R. M. Nieminen, and K. Niemelä, Phys. Rev. B **69**, 153101 (2004).
[58] T. Soda, Y. Kitagawa, T. Onishi, Y. Takano, Y. Shigeta, H. Nagao, Y. Yoshioka, and K. Yamaguchi, Chem. Phys. Lett. **319**, 223 (2000).
[59] A. J. Cohen, P. Mori-Sánchez, and W. Yang, Science **321**, 792 (2008).
[60] T. Chwiej, S. Bednarek, B. Szafran, J. Adamowski, and F. M. Peeters, Phys. Rev. B **73**, 075422 (2006).
[61] M. Ishizuki, H. Takemiya, T. Okunishi, K. Takeda, and K. Kusakabe, Phys. Rev. B **85**, 155316 (2012).
[62] J. Gräfenstein, E. Kraka, M. Filatov, and D. Cremer, Int. J. Mol. Sci. **3**, 360 (2002).
[63] K. Huang and A. Rhys, Proc. R. Soc. London, Ser. A **204**, 406 (1950).
[64] S.-Y. Lee, M. Widmann, T. Rendler, M. W. Doherty, T. M. Babinec, S. Yang, M. Eyer, P. Siyushev, B. J. Hausmann, M. Loncar *et al.*, Nat. Nanotechnol. **8**, 487 (2013).
[65] T. E. Sharp and H. M. Rosenstock, J. Chem. Phys. **41**, 3453 (1964).
[66] A. Alkauskas, B. B. Buckley, D. D. Awschalom, and C. G. V. de Walle, New J. Phys. **16**, 073026 (2014).
[67] J. A. B. Ferreira, A. Sanchez-Coronilla, D. M. Togashi, H. Ferreira, J. R. Ascenso, and S. M. B. Costa, Chem. Phys. **273**, 39 (2001).